Wind-Driven Motion near a Shelf–Slope Front[1]

HSIEN WANG OU

Lamont-Doherty Geological Observatory, Columbia University, Palisades, NY 10964

(Manuscript received 18 July 1983, in final form 3 November 1983)

ABSTRACT

A two-dimensional, two-layered frontal system is used to examine the wind-driven motion near a shelf–slope front. In the linear regime, the along-frontal current is characterized by barotropic perturbations. The front is dynamically passive and displaced according to purely kinematic constraints. The nonlinear solution shows that, even for a relatively small Rossby number, the frontal response to the oppositely directed along-frontal winds is highly asymmetric. When the wind is such that it forces surface water offshore, the model predicts ridging of the frontal interface, resembling some hydrographic observations. The model results suggest that the topographic shoaling of the deep onshore flow causes the generation of a cyclonic shear which, in a nonlinear regime, produces the observed ridging through geostrophic balance. It is reasoned that the increased entrainment above the pycnocline ridge could cut off the offshore shelf water and result in its export to the slope water regime. On the other hand, the apparent rigidity of the front as the surface water moves shoreward suggests a relative ineffectiveness for the surface slope water to penetrate through the frontal zone and contribute to mass or property balances on the shelf.

1. Introduction

During the winter season, shelf water is well mixed in the Middle Atlantic Bight because of intensified wind stirring and surface cooling. It is separated from a slightly stratified slope water by a rather sharp transition region near the shelf break called the shelf–slope front (Fig. 1). Although the shelf water is both colder and fresher than the slope water, salinity variation dominates the density field, making the shelf water the less dense of the two water masses—the front thus generally slopes upward offshore, with a mean slope of the order of 2×10^{-3}.

The shelf–slope front is observed to exhibit large spatial and temporal variations which have been attributed to both external forcings and internal instabilities. One external forcing mechanism that can be clearly seen from satellite infrared images is the impingement of warm core rings that greatly distort the front and frequently entrain the shelf water, forming streaks and filaments. Less obvious perhaps are the frontal motions driven by wind. Nevertheless, Flagg (1977) has documented one such example in which the surface front is displaced offshore at the onset of a strong southwesterly wind.

Direct current measurements show that wind causes much of the current variability in the shallower shelf water (Beardsley and Boicourt, 1981). The wind effect diminishes offshore because of the increase of both water depth and interference of the offshore oceanic forcing. But the current records obtained during the NSFE79 experiment (Beardsley *et al.*, 1983) show definite wind-driven components even at the outer moorings situated within the frontal zone.

Since surface wind contributes to the frontal variability, it is of practical importance to understand how a front responds to such a forcing. This however has been an area noticeably lacking in theoretical studies. Some published works (e.g., Csanady, 1978; Hsueh and Cushman-Roisin, 1982) deal with the wind effect on the geostrophically adjusted state of an initially vertical front and apply only at the formation stage of the shelf–slope front. In this paper, I attempt instead an examination of the response of an equilibrium front to wind forcing, which might help to interpret some observed frontal variability.

The model is formulated in Section 2, followed by some discussions of the linear regime in Section 3. The nonlinear problem is solved numerically in Section 4 for a suddenly imposed wind. A summary of the model results and some of their implications are presented in Section 5.

2. The model

The model configuration is schematically shown in Fig. 2 where the front is approximated by a two-dimensional (y, z) density interface that separates two homogeneous layers, designated layer 1 and 2. The front intersects the bottom at $y = L$ near the shelf break, and slopes upward offshore until it reaches the base of the surface mixed layer at $y = M$ at which

[1] Lamont-Doherty Geological Observatory Contribution Number 3632.

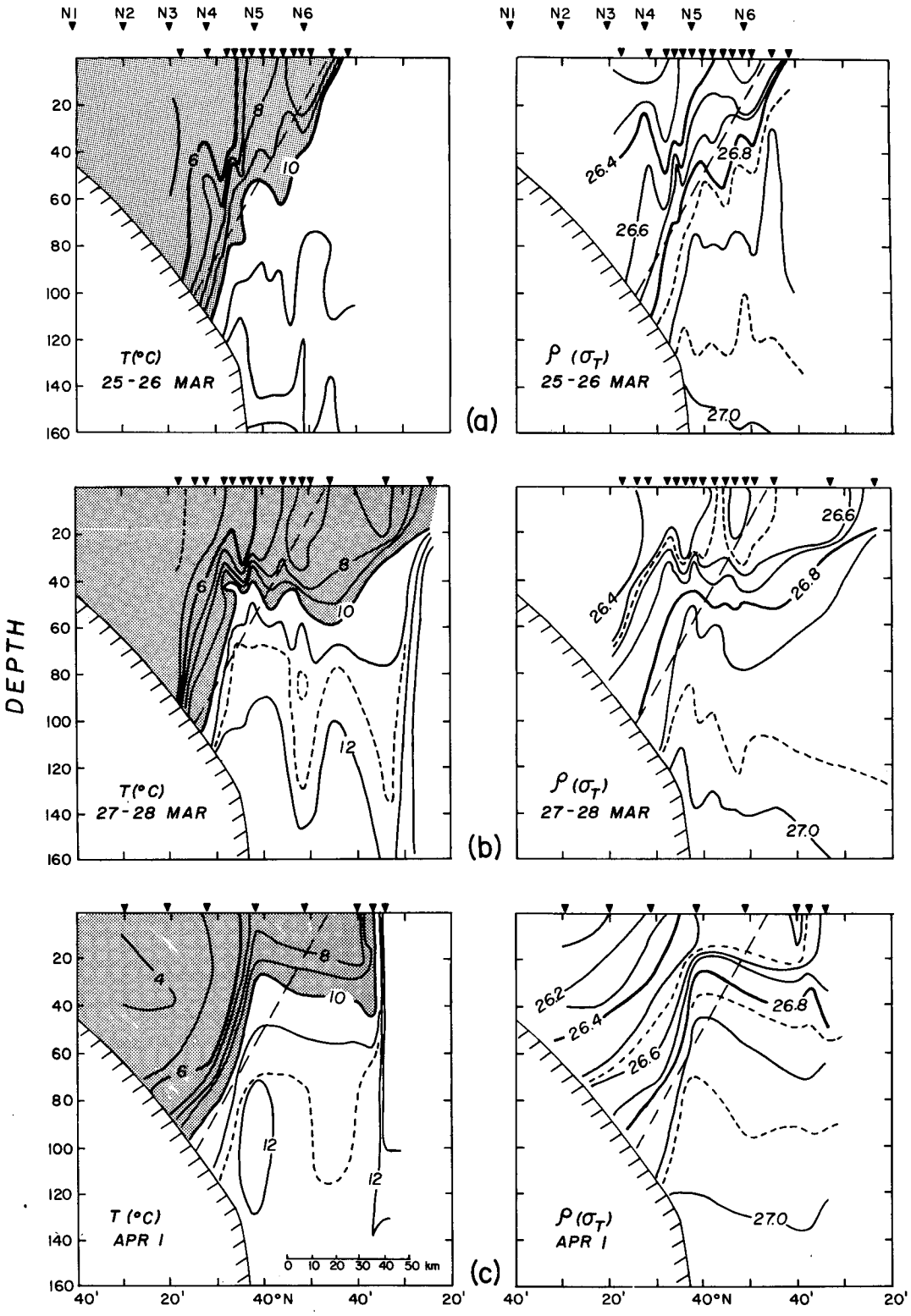

FIG. 1. Temperature and density sections across the New England shelf-slope front (adapted from Marra *et al.*, 1982). The dashed line indicates the historical frontal position according to Wright (1976).

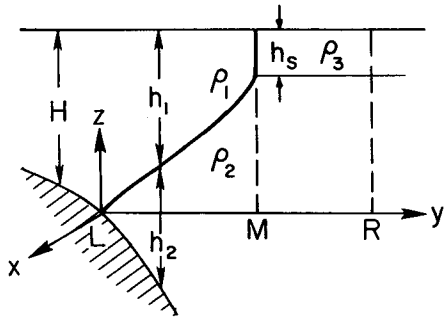

FIG. 2. The model configuration.

point it becomes vertical. For both the mean state in the linear model and the initial state in the nonlinear model L equals zero. The vertical interface at $y = M$ will be referred to as the surface front and the region between $y = L$ and M is called the frontal zone. Although the frontal zone is the region of primary interest in this study, a wider region extending seaward of the frontal zone (to $y = R$) will be needed in numerical calculations of the nonlinear solution to facilitate a more realistic implementation of the offshore boundary condition, in which case a two-layer structure will be assumed seaward of the frontal zone as indicated in the figure. In our terminology, the x and y directions will be called along- and cross-frontal respectively.

Since in a two-dimensional model with along-frontal uniformity, the along-frontal wind is the dominant component that drives the flow (Gill, 1982, p. 399), I will limit the discussion to this component of the wind forcing. Coupled with the observation that the along-frontal current is generally much greater than the cross-frontal current for the time scale that we are concerned with (i.e., days), the along-frontal current is assumed geostrophic. This implies that the along-frontal current is vertically uniform within both layers and satisfies the Margules equation across the frontal interface,

$$f(u_1 - u_2) = -\delta g' h_{1y}, \tag{2.1}$$

where the letter subscript, as will be used throughout this paper, represents a partial derivative. In (2.1) f is the Coriolis parameter, g' the reduced gravity based on the density difference between layer 1 and 2, and δ has the value of 1 within the frontal zone but equals $(\rho_2 - \rho_3)/(\rho_2 - \rho_1)$ seaward of the frontal zone. Since the sea surface has a vertical displacement much smaller than that of the frontal interface, it is treated as rigid. With the additional assumptions of an inviscid, adiabatic and Boussinesq fluid, and an implicit presence of coast, the remaining governing equations are given by

$$\frac{d}{dt} u_1 - fv_1 = \frac{\tau}{h_1}, \tag{2.2}$$

$$\frac{d}{dt} u_2 - fv_2 = 0, \tag{2.3}$$

$$(h_1 v_1)_y + h_{1t} = 0, \tag{2.4}$$

$$h_1 v_1 + h_2 v_2 = 0, \tag{2.5}$$

$$h_1 + h_2 = H, \tag{2.6}$$

where v_1 and v_2 are the vertically averaged cross-frontal flows within the respective layer, τ is the along-frontal wind stress and H is the total water depth. The six variables $(u_1, v_1, u_2, v_2, h_1, h_2)$ are then determined by the six equations (2,1) through (2.6).

Since the currents are predominantly wind-driven, they are nondimensionalized by the scales

$$(u^*, v^*) \equiv \frac{\tau^*}{H_0}\left(T, \frac{1}{f}\right),$$

where τ^* is the characteristic scale of the wind stress magnitude, H_0 is the water depth at $y = 0$ and T is the time scale. With the further scalings that $(z^*, y^*) \equiv (H_0, g'H_0/fu^*)$, the nondimensionalized variables satisfy the following equations:

$$u_1 - u_2 = -\delta h_{1y}, \tag{2.7}$$

$$u_{1t} + \epsilon v_1 u_{1y} - v_1 = \frac{\tau}{h_1}, \tag{2.8}$$

$$u_{2t} + \epsilon v_2 u_{2y} - v_2 = 0, \tag{2.9}$$

$$\epsilon(h_1 v_1)_y + h_{1t} = 0, \tag{2.10}$$

$$h_1 v_1 + h_2 v_2 = 0, \tag{2.11}$$

$$h_1 + h_2 = H, \tag{2.12}$$

where $\epsilon = u^*/(fy^*) = (u^*)^2/(g'H_0)$ is the Rossby number, or the internal Froude number according to our scaling.

3. The linear regime

For $\epsilon \ll 1$, Eq. (2.10) implies that the vertical displacement of the front is small. This is expected since the front is stiffer for a weaker forcing or stronger stratification. This allows us to decompose the upper-layer depth into its mean value (denoted by an overbar) and a small perturbation (denoted by a prime),

$$h_1 = \bar{h}_1 + \epsilon h_1'. \tag{3.1}$$

Similar decomposition can be done on the flow fields,

$$u_1 = \bar{u}_1 + u_1', \text{ etc.}, \tag{3.2}$$

although the perturbation is not necessarily small compared with the mean.

Substituting (3.1) and (3.2) into (2.7) yields

$$u_1' \approx u_2', \tag{3.3}$$

i.e., as a consequence of the small frontal displacement, the perturbation in the along-frontal current is barotropic. The front thus plays no dynamical role in the wind-driven flow field, and its vertical displacement

is determined through the kinematic constraint (2.10). Subject to (3.3), the perturbation fields can be easily solved, and are presented in Appendix A.

In an adiabatic model with no mixing, the surface front is simply advected by the cross-frontal flow, but that leads to gravitational instability when the denser surface slope water is advected shoreward over the less dense shelf water. The linear solution thus breaks down in this case near the surface front. To resolve this problem and also to examine the case when ϵ is not small, we have to solve the nonlinear problem.

4. The nonlinear solution

Numerical means are employed to solve the full set of equations, (2.7) through (2.12), without dropping the nonlinear terms. To reduce the set, we first derive, from (2.9), (2.11) and (2.12), that

$$u_{2t} = -\frac{V_1}{H - h_1}(1 - \epsilon u_{2y}), \tag{4.1}$$

where $V_1 \equiv h_1 v_1$ is the cross-frontal transport in the upper layer. Taking the time derivative of (2.7) and using (2.10) and (4.1) yield

$$u_{1t} = -\frac{V_1}{H - h_1}(1 - \epsilon u_{2y}) + \delta\epsilon V_{1yy}. \tag{4.2}$$

while taking the y derivative of (2.7) leads to

$$u_{1y} = u_{2y} - \delta h_{1yy}. \tag{4.3}$$

Substituting (4.2) and (4.3) into (2.8), we arrive at

$$V_{1yy} - \frac{V_1}{h_1}\left[h_{1yy} + \frac{H}{\delta\epsilon(H - h_1)}(1 - \epsilon u_{2y})\right] = \frac{\tau}{\delta\epsilon h_1}. \tag{4.4}$$

This is a diagnostic equation for V_1 in terms of h_1 and u_2 which can be calculated through the prognostic equations (2.10) and (4.1). The remaining variables can be easily calculated once V_1, h_1 and u_2 are obtained.

The numerical procedure involves solving the above equations over a variable domain encompassing the frontal zone, the boundaries of which have to be tracked at each time step. The inshore boundary of the domain is set at $y = L$ where the front intersects the bottom, and the offshore boundary is set at $y = R$ such that the width of the domain $(R - L)$ is, for practical reasons, a fixed multiple of the frontal zone width $(M - L)$.

The boundary condition at $y = L$ can be rigorously formulated. By definition, this is where $h_1 = H(L)$, and, from (2.11), we require that $V_1 = 0$. For the boundary condition on u_2, we integrate the momentum equation (2.9) in time to give $u_2 = L/\epsilon$ which has been assumed to vanish initially for simplicity. The boundary itself is moving according to the kinematic relation

$$h_{2t} + L_t h_{2y} = 0, \tag{4.5}$$

or, using (2.10) and (2.12),

$$L_t = -\frac{\epsilon V_{1y}}{(H - h_1)_y}. \tag{4.6}$$

To derive the boundary condition at $y = R$, we assume that it is far enough away from the frontal zone and into the open ocean that the asymptotic boundary condition $h = h_s$ applies, where h_s is some nominal depth of the surface mixed layer. Eq. (2.10) then implies that $(V_1/h_1)_y = 0$. For the boundary condition on u_2, we must distinguish between the case of negative and positive wind stress. In the case of negative wind stress, this boundary is advected offshore, encroaching upon a region previously lying outside the domain of integration. Because of the great water depth there, the stretching mechanism is negligible in generating relative vorticity, which is assumed to be zero initially for the sake of simplicity; we therefore impose the boundary condition that $u_{2y} = 0$. For the case of positive wind stress, this boundary is advected shoreward, taking on points previously lying within the domain of integration; u_2 therefore need not be specified.

To facilitate the numerical calculation, we first transform the (y, t) coordinate system to the (ζ, t) system, where $\zeta \equiv (y - L)/(M - L)$, such that the frontal zone occupies a fixed domain $\zeta \in (0, 1)$, and we then finite-difference the resulting equations within the domain of integration $(0, \zeta_R)$ where ζ_R is a fixed number greater than 1. The direct method of Lindzen and Kuo (1969) is used to solve the diagnostic equation of V_1, and the Lax-Wendroff scheme is used to calculate h_1 and u_2 from their prognostic equations. Readers are referred to Appendix B for the details of the numerical algorithm.

In the examples shown below, I use $h_s = 0.2$ and $\epsilon = 0.2$. The values are chosen to correspond to observed values (see Section 5). The bottom topography, shown by the dashed line in Fig. 3a in greatly reduced vertical scale, has the profile of a hyperbolic tangent to simulate that near a continental margin. The initial state is characterized by a straight front that spans a unit distance and a motionless lower layer. The numerical solution is calculated for a suddenly imposed along-frontal wind stress of unit magnitude. A grid spacing of 0.025 and a time step of 0.01 are used in all the numerical runs. Increasing values of ζ_R are used in each case until the solution has sufficiently converged within the frontal zone. It turns out that $\zeta_R = 2$ is sufficient for the case of negative wind stress while $\zeta_R = 4$ is needed for the case of positive wind stress. Since the solution in the frontal zone is found to be insensitive to the variation of δ, an arbitrary value of 0.5 is used in the following presentations.

Figure 3a shows the front at four successive time intervals ($t = 0$, 1, 2 and 3) for the case of a negative

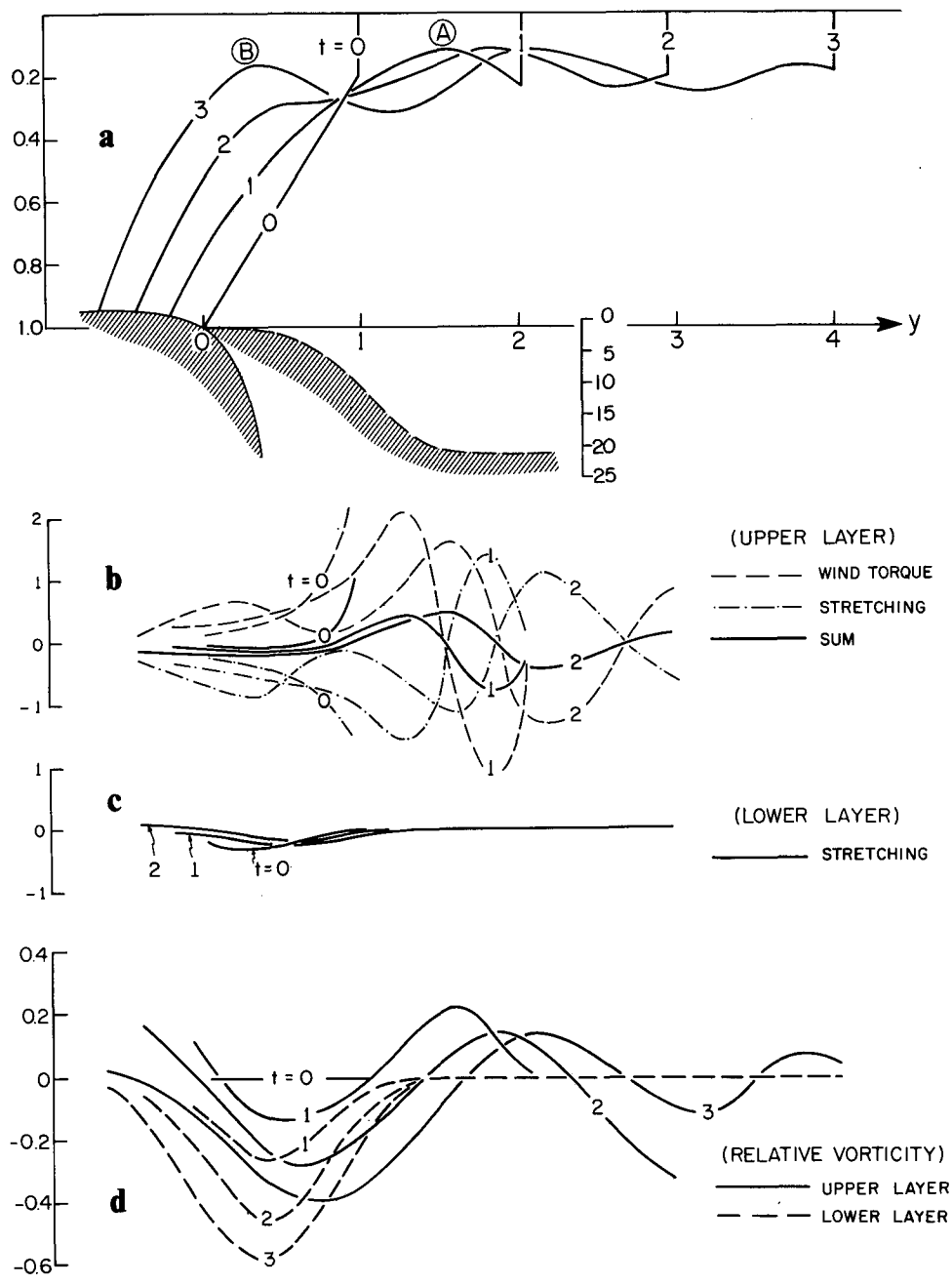

FIG. 3. (a) The frontal shape for $\tau = -1$ at $t = 0$, 1, 2 and 3. The bottom topography has the profile of a hyperbolic tangent and is shown by the dashed line with greatly reduced vertical scale. Capital letters A and B designate the primary and secondary ridge respectively. Vorticity input terms and their sum in (b) the upper layer and (c) the lower layer at $t = 0$, 1 and 2. (d) Relative vorticities in the two layers at $t = 0$, 1, 2 and 3.

wind stress. As expected, the surface front is advected offshore, accompanied by a shoreward motion in the lower layer. But in addition to the general flattening of the front, the frontal interface exhibits some degree of convolution. Of particular interest is the early appearance of a ridge just shoreward of the surface front (indicated by the letter A), accompanied by minor offshore undulations as time progresses, and the later appearance of another ridge closer to shore (indicated by the letter B). The two ridges will, for convenience, be referred to as primary and secondary, respectively. The designation only refers to their time sequence in

occurrence and is not indicative of their relative amplitudes. These features can best be explained by the vorticity balance derived from (2.8) through (2.10),

$$\frac{d\Omega_1}{dt} = \frac{\Omega_1}{h_1}\frac{dh_1}{dt} - \epsilon\left(\frac{\tau}{h}\right)_y, \tag{4.7}$$

$$\frac{d\Omega_2}{dt} = \frac{\Omega_2}{h_2}\frac{dh_2}{dt}, \tag{4.8}$$

where $\Omega_1 \equiv 1 - \epsilon u_{1y}$ and $\Omega_2 \equiv 1 - \epsilon u_{2y}$ are the total vorticities in the two layers. The two terms on the right hand side of (4.7) are referred to as the "stretching" and "wind torque" term, respectively, with their obvious physical connotations. Only the stretching term contributes to the vorticity change in the lower layer. Using the Margules equation (2.7), we derive that

$$h_{1yy} = (\Omega_1 - \Omega_2)/\delta\epsilon, \tag{4.9}$$

i.e., the curvature of the frontal interface is proportional to the vorticity shear, a relation that will be invoked in the following discussions.

I have plotted the vorticity input terms and the relative vorticities of the two layers in Fig. 3b through 3d. Initially, the front slopes upward monotonically, hence a positive wind torque term; and the upward motion at the frontal interface gives a negative stretching term. The wind torque term dominates near the surface front and generates the positive relative vorticity observed at $t = 1$. In the lower layer, the relative vorticity remains negligible near the surface front on account of the inefficiency of the stretching mechanism (because of the great water depth). The resulting cyclonic shear, in accordance with (4.9), causes the primary ridge observed in Fig. 3a. Seaward of the ridge, the pycnocline slopes downward, the wind torque term becomes negative and again, because of its dominance over the stretching term near the surface front, tends to generate anticyclonic shear and hence a negative curvature in the pycnocline. The process continues in time and results in the observed undulations seaward of the primary ridge. Since the magnitude of the wind torque term is proportional to the pycnocline slope, which generally diminishes as the front is spreading out, its effectiveness in generating vorticity diminishes accordingly—the primary ridge and the frontal undulations thus reach some finite amplitude and then taper off in time.

This is in sharp contrast to the secondary ridge which appears to be unlimited in its magnitude. In fact, the secondary ridge reaches the surface before the next time interval ($t = 4$) when the solution breaks down. By comparing Figs. 3a and 3d, it is seen that the secondary ridge is dominated by the negative relative vorticity generated in the lower layer as the deeper fluid is forced up the topographic slope. Since this vorticity-generating mechanism is strongly tied to the topography and is not overly dependent on the frontal shape, the ridge occurs near the shelf break where the flow has a maximum convergence and its amplitude grows in time. To demonstrate this topographic effect further, the solution for a flat bottom is plotted in Fig. 4, which clearly shows the absence of the secondary ridge.

From the above discussion, it is seen that variation of the initial frontal shape would affect considerably the efficiency of the wind torque in generating the primary ridge, but not so much the topographic effect in generating the secondary ridge. In addition, presence of nonzero relative vorticities within either layer at $t = 0$ can enhance or diminish the ridging feature as the vortex elements are advected by the cross-frontal flow. The effect, however, is rather straightforward and needs not be discussed here.

The solution for the positive wind is shown in Fig. 5. Again, as expected, the surface water is advected shoreward while the deeper fluid is moving offshore. The cross-frontal flow is increasingly constrained as the frontal zone narrows and the front appears to be rather rigid compared with the negative wind case when the lighter shelf water is spreading offshore above the denser slope water. This asymmetric response in the cross-frontal flow necessarily leads to the asymmetry in the along-frontal flow. Since in the case of positive wind stress, the cross-frontal flow is severely constrained, the bulk of the wind stress is used to accelerate

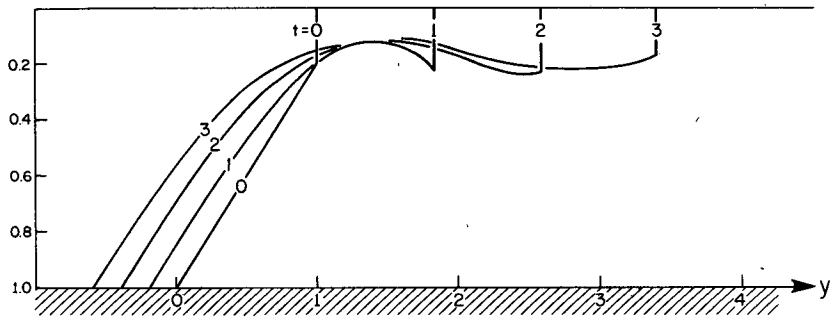

FIG. 4. As in Fig. 3a, but for a flat bottom.

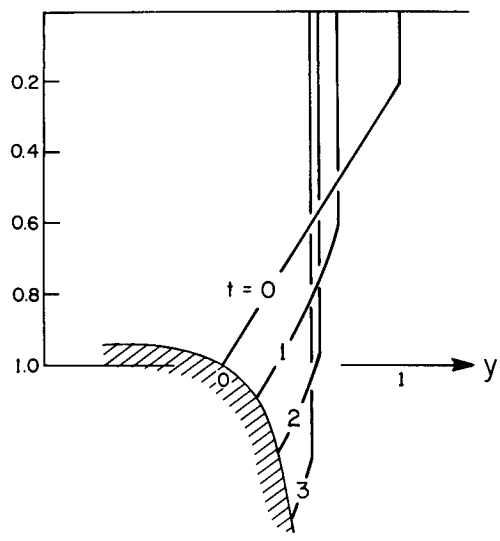

FIG. 5. As in Fig. 3a, but for $\tau = 1$.

the along-frontal flow which then attains a much greater amplitude (averaged within the frontal zone) than in the negative wind case when much of the wind stress is balanced by the Coriolis force associated with the large offshore flow. Also notice that the surface front deepens as it is advected shoreward, again in sharp contrast to the negative wind case when the surface front maintains more or less a constant depth.

5. Summary and discussion

We have examined the wind-driven motion near a two-dimensional, two-layered frontal system. In the linear regime when the vertical displacement of the frontal interface is small in comparison with the upper-layer depth, the perturbation in the along-frontal current is barotropic—the front plays no dynamical role in determining the wind-driven flow fields, and is displaced according to purely kinematic constraints. The nonlinear solution shows that even for a relative small Rossby number, the frontal response to the oppositely directed along-frontal wind is highly asymmetric. The asymmetric behavior stems from the fact that the cross-frontal flow is more constrained when the frontal zone narrows, as in contrast to the opposite case when the surface water is spread offshore above the denser fluid. The reduced cross-frontal flow allows for a more efficient forcing by wind on the along-frontal current, which generally attains a much greater amplitude within the frontal zone.

Of particular interest in the numerical solution is the ridging of the frontal interface as the surface water is advected offshore, in resemblance to that observed in Fig. 1c. Examination of the wind data (see Fig. 1 of Beardsley *et al.*, 1983) prior to the hydrographic measurements shows that the wind was from the southwest, as required by the model. The wind stress has a magnitude of approximately 2 dyn cm^{-2}. With the time scale set at 1 day, the scale of the along-frontal current is 20 cm s^{-1}. If we identify the front in Fig. 1 as the region sandwiched between the isopycnals 26.6 and 26.8 σ_T, the reduced gravity g' is 0.2 cm s^{-2}. With $H_0 = 100$ m, the crossfrontal scale y^* is 10 km, and the Rossby number is 0.2 which is the value used in our numerical calculations.

Although both the wind torque acting on the upper layer and the topographic constraint acting on the lower layer can generate the cyclonic shear needed for the ridging of the frontal interface, the ridges produced by the two mechanisms behave quite differently. In general, the ridge produced by the topographic mechanism is less sensitive to the frontal shape, is more strongly tied to the shelf break, and attains a much greater amplitude. The model results thus suggest that the topographic mechanism is the likely one that causes the observed ridging.

The numerical solution breaks down when the top of the ridge reaches the surface, resulting in an infinite cross-frontal flow there. It is reasoned, however, that before the pycnocline reaches the surface, the increased entrainment across the ridged interface would cut off the offshore shelf water and result in its exportation to the slope water regime. Surface temperature measurements have frequently shown cold shelf water separated by warm bands near the shelf break (Houghton, personal communication, 1983), in agreement with this deduction concerning the model results. On the other hand, the relative rigidity of the front when the surface water is advected shoreward suggests a relative ineffectiveness for the surface slope water to penetrate through the frontal zone and contribute to mass or property balances on the shelf.

Acknowledgments. I want to thank Kenneth H. Brink and many of my colleagues for reading and commenting on the manuscript. This work is supported by the National Science Foundation under Grant OCE 81-17579 and the Department of Energy under Grant DE-AC02-76EV02185FX.

APPENDIX A

The Linear Solution

Let the perturbation in the along-frontal current be denoted by u'; then the perturbation fields satisfy, to the lowest order, the following equations:

$$u'_t - v'_1 = \tau'/\bar{h}_1, \tag{A1}$$

$$u'_t - v'_2 = 0, \tag{A2}$$

$$(\bar{h}_1 v'_1)_y + h'_{1t} = 0, \tag{A3}$$

$$\bar{h}_1 v'_1 + \bar{h}_2 v'_2 = 0. \tag{A4}$$

The solution is easily obtained,

$$u' = \int \frac{\tau'}{H}\, dt, \tag{A5}$$

$$v_2' = \frac{\tau'}{H}, \tag{A6}$$

$$v_1' = -\frac{\bar{h}_2}{\bar{h}_1 H}\tau', \tag{A7}$$

$$h_1' = \int \left(\frac{\bar{h}_2 \tau'}{H}\right)_y dt. \tag{A8}$$

Although the vertically averaged flow v_1' vanishes at $y = 0$ where the lower layer ceases to exist, observation over the shelf shows that the cross-shelf flow is dominated by oppositely directed flows in the upper and lower portion of the water column (Beardsley and Boicourt, 1981, p. 219). To accomodate this observation, a simple refinement is made to divide the upper layer into a surface mixed layer and an interior region. Let them be denoted by the subscripts "S" and "I," respectively, then

$$v_I' = v_2', \tag{A9}$$

since they satisfy the same equation (A2), and v_S' can be determined from the requirement of zero cross-frontal mass flux,

$$\bar{h}_S v_S' + (H - \bar{h}_S)v_2' = 0, \tag{A10}$$

or

$$v_S' = -\frac{H - \bar{h}_S}{H\bar{h}_S}\tau'. \tag{A11}$$

APPENDIX B

The Numerical Algorithm

The following derivations are for the case of negative wind stress when the surface water is advected offshore. For the case of a positive wind stress, the derivations are identical except for the treatment of the offshore boundary condition on u_2 which will be presented at the end.

We first summarize the governing equations below:

$$V_{1yy} - \frac{V_1}{h_1}\left[h_{1yy} + \frac{H}{\delta\epsilon(H - h_1)}(1 - \epsilon u_{2y})\right] = \frac{\tau}{\delta\epsilon h_1}, \tag{B1}$$

$$h_{1t} = -\epsilon V_{1y}, \tag{B2}$$

$$u_{2t} = -\frac{V_1}{H - h_1}(1 - \epsilon u_{2y}), \tag{B3}$$

with the boundary conditions that

$$V_1 = 0, \quad h_1 = H(L), \quad u_2 = L/\epsilon, \quad \text{at} \quad y = L, \tag{B4}$$

$$(V_1/h_1)_y = 0, \quad h_1 = h_s, \quad u_{2y} = 0, \quad \text{at} \quad y = R. \tag{B5}$$

The frontal boundaries are moving according to

$$L_t = -\epsilon[V_{1y}/(H - h_1)_y]_{y=L}, \tag{B6}$$

$$M_t = \epsilon[V_1/h_1]_{y=M}. \tag{B7}$$

If we transform the coordinate system (y, t) to (ζ, t) where $\zeta \equiv (y - L)/(M - L)$, then the frontal zone occupies the fixed domain $\zeta \in (0, 1)$. The domain of integration is $(0, \zeta_R)$ with ζ_R a number greater than 1. The derivatives are transformed according to

$$\partial_y = \frac{1}{W}\partial_\zeta, \tag{B8}$$

$$\partial_y^2 = \frac{1}{W^2}\partial_\zeta^2, \tag{B9}$$

$$\partial_t = \partial_t + E\partial_\zeta, \tag{B10}$$

where $W \equiv M - L$ is the width of the frontal zone and

$$E \equiv -\frac{1}{W}[(1 - \zeta)L_t + \zeta M_t].$$

Substituting (B8) through (B10) into (B1) through (B7), we derive that

$$V_{1\zeta\zeta} - \frac{V_1}{h_1}\left[h_{1\zeta\zeta} + \frac{W^2 H}{\delta\epsilon(H - h_1)}\left(1 - \frac{\epsilon}{W}u_{2\zeta}\right)\right] = \frac{W^2\tau}{\delta\epsilon h_1}, \tag{B11}$$

$$h_{1t} = -Eh_{1\zeta} - \frac{\epsilon}{W}V_{1\zeta}, \tag{B12}$$

$$u_{2t} = -Eu_{2\zeta} - \frac{V_1}{H - h_1}\left(1 - \frac{\epsilon}{W}u_{2\zeta}\right), \tag{B13}$$

with the boundary conditions that,

$$V_1 = 0, \quad h_1 = H(0), \quad u_2 = L/\epsilon, \quad \text{at} \quad \zeta = 0, \tag{B14}$$

$$(V_1/h_1)_\zeta = 0, \quad h_1 = h_s, \quad u_{2\zeta} = 0, \quad \text{at} \quad \zeta = \zeta_R. \tag{B15}$$

The frontal boundaries are moving according to

$$L_t = -\epsilon[V_{1\zeta}/(H - h_1)_\zeta]_{\zeta=0}, \tag{B16}$$

$$M_t = \epsilon[V_1/h_1]_{\zeta=1}. \tag{B17}$$

The finite differenced equation of (B11) is solved by the direct method of Lindzen and Kuo (1969), and the Lax-Wendroff scheme is used to integrate (B12) and (B13) in time from their initial values.

For the case of a positive wind stress, a backward difference scheme is used for $u_{2\zeta}$ at the end point ζ_R which eliminates the need for a boundary condition there.

REFERENCES

Beardsley, R. C., and W. C. Boicourt, 1981: On estuarine and continental-shelf circulation in the Middle Atlantic Bight. *Evolution of Physical Oceanography*, B. A. Warren and C. Wunsch, Eds., The MIT Press, 198–233.

——, C. A. Mills, J. A. Vermersch, W. S. Brown, N. Pettigrew, J. Irish, S. Ramp, R. Schlitz and B. Butman, 1983: Nantucket Shoals Flux Experiment (NSFE79). Part 2: Moored array data report, WHOI Tech. Rep., in preparation.

Csanady, G. T., 1978; Wind effects on surface to bottom fronts. *J. Geophys. Res.*, **83,** 4633–4640.

Flagg, C. N., 1977: The kinematics and dynamics of the New England continental shelf and shelf-slope front. Doctoral dissertation, MIT/WHOI Joint Program, 207 pp.

Gill, A. E., 1982: *Atmosphere-Ocean Dynamics.* Academic Press, 662 pp.

Hsueh, Y., and B. Cushman-Roisin, 1982: On the formation of surface to bottom fronts over steep topography. *J. Geophys. Res.*, **88,** 743–750.

Lindzen, R. S., and H. L. Kuo, 1969: A reliable method for the numerical integration of a large class of ordinary and partial differential equations. *Mon. Wea. Rev.*, **96,** 732–734.

Marra, J., R. W. Houghton, D. C. Boardman and P. J. Neale, 1982: Variability in surface chlorophyll *a* at a shelf-break front. *J. Mar. Res.*, **40,** 575–591.

Wright, W. R., 1976: The limits of shelf water south of Cape Cod, 1941 to 1972. *J. Mar. Res.*, **34,** 1–14.